Fibrin Clot Structure and Mechanics Associated with Specific Oxidation of Methionine Residues in Fibrinogen

Katie M. Weigandt,[†] Nathan White,[§] Dominic Chung,[‡] Erica Ellingson,[†] Yi Wang,[||] Xiaoyun Fu,[¶||] and Danilo C. Pozzo[†*]

[†]Department of Chemical Engineering, [‡]Department of Biochemistry, [§]Division of Emergency Medicine, and [¶]Division of Hematology, University of Washington, Seattle, Washington; and [||]Puget Sound Blood Center Research Institute, Seattle, Washington

ABSTRACT Using a combination of structural and mechanical characterization, we examine the effect of fibrinogen oxidation on the formation of fibrin clots. We find that treatment with hypochlorous acid preferentially oxidizes specific methionine residues on the α, β, and γ chains of fibrinogen. Oxidation is associated with the formation of a dense network of thin fibers after activation by thrombin. Additionally, both the linear and nonlinear mechanical properties of oxidized fibrin gels are found to be altered with oxidation. Finally, the structural modifications induced by oxidation are associated with delayed fibrin lysis via plasminogen and tissue plasminogen activator. Based on these results, we speculate that methionine oxidation of specific residues may be related to hindered lateral aggregation of protofibrils in fibrin gels.

INTRODUCTION

Fibrinogen is a 340 kDa plasma protein and the precursor to fibrin, which is the primary structural component of blood clots and is critical for hemostasis after injury (1). In healthy individuals, fibrinogen is present in the blood at concentrations of 2–4 mg/mL. Upon injury, a series of biochemical processes occur that result in the local release and activation of thrombin. This enzyme cleaves two short peptide sequences (fibrinopeptides A and B) from fibrinogen and converts it to fibrin. The removal of these polypeptides exposes binding sites and drives the self-assembly of fibrin molecules into a half-staggered, two-stranded array termed a protofibril. Fibrinogen has two αC domains that normally self-associate with the central domain of the monomer. Upon conversion to fibrin, the αC domains dissociate and are thought to play a role in the lateral aggregation of protofibrils leading to the formation of coarse fibers (2,3). However, the extent of lateral aggregation is also affected by solution conditions and by modifications to the fibrinogen monomer (2,3).

Many disease states are associated with abnormal fibrin clot structure. Blood clots that form in thrombotic diseases such as ischemic stroke, diabetes, and renal impairment tend to have thin fibrin fibers, reduced clot porosity, and delayed fibrinolysis relative to healthy patients (4–6). However, the mechanisms underlying these structural changes during disease remain unknown. Heterogeneous fibrin clot formation can be the result of genetic or biochemical modifications that may occur during protein formation or subsequently during circulation. Known modifications to fibrinogen include degradation of the carboxy terminal groups of the αA and γ chains, glycation of lysine residues in diabetes patients, and partial oxidation of methionine residues, each of which can affect polymerization (7). By gaining a better understanding of the impact of molecular changes associated with disease-induced coagulopathies, we may be able to develop medical intervention strategies that prevent complications related to altered coagulation.

Fibrinogen is more susceptible to oxidation than most other plasma proteins, and several coagulation factors, including fibrinogen, are sensitive to hypochlorite oxidation (8,9). Hypochlorous acid is generated in vivo locally at sites of injury, infection, or inflammation as part of the natural immune response (10). Neutrophils, a type of white blood cell, produce high local concentrations of hypochlorous acid in vivo through the reaction of hydrogen peroxide and Cl^- via the enzyme myeloperoxidase (11). Hypochlorous acid oxidizes methionine to form methionine sulphoxide with a high second-order rate constant (k) of 3.8×10^7 $M^{-1}s^{-1}$, and thus this reaction occurs preferentially over the oxidation of most other amino acids (12). Methionine oxidation by hypochlorous acid has been shown to inhibit important regulatory coagulation proteins, including activated protein C and thrombomodulin (13,14). In such cases, the deactivation of these proteins has been traced to the oxidation of individual methionine residues. In fibrinogen, oxidation with hypochlorous acid has been shown to reduce lateral aggregation and to trigger altered lysis behavior in fibrin clots (15). Other studies have demonstrated that restricting lateral aggregation, which promotes the formation of dense fibrous gels, is linked to delayed clot lysis due to impaired diffusion of plasmin through smaller pores (5,16).

In this study, we examine the effect of oxidation with hypochlorous acid on the structural, mechanical, and lytic properties of fibrin gels. A combination of turbidity, small-angle neutron scattering (SANS), and scanning electron microscopy (SEM) is used to characterize the structure of the fibrin gels. Shear rheology is utilized to measure the

Submitted August 29, 2012, and accepted for publication October 24, 2012.

*Correspondence: dpozzo@u.washington.edu

Editor: Fazoil Ataullakhanov.

0006-3495/12/12/2399/9 $2.00

http://dx.doi.org/10.1016/j.bpj.2012.10.036

linear and nonlinear bulk rheological properties of fully formed fibrin gels, and to track the dissolution of gels during tissue plasminogen activator (tPA) and plasminogen-induced clot lysis. The results of this work are discussed with respect to several studies that link conformational changes in the αC domain to inhibition of lateral aggregation in fibrin clots.

MATERIALS AND METHODS

Sample preparation

Human fibrinogen (plasminogen and von Willebrand depleted) and human-α-thrombin were purchased from Enzyme Research Laboratories (South Bend, IN). The fibrinogen was defrosted to 37°C and dialyzed to achieve a 99.9% exchange into a buffer solution of 0.14 M NaCl and 44 mM Hepes titrated to pH 7.4 in deionized H_2O. The fibrinogen solution was filtered through 0.45 μm PVDF filters and the concentration was determined by UV-Vis spectroscopy at $\lambda = 280$ nm with an extinction coefficient of 1.6 mg $mL^{-1}cm^{-1}$ (17).

The fibrinogen was oxidized with 50 or 150 μmol HOCl/g fibrinogen and incubated for 1 h at 37°C. The oxidation reaction was quenched with a 10× molar excess of L-methionine. The nonoxidized sample was made to have the same composition as the 50 μmol sample by addition of prequenched HOCl and methionine. After oxidation, the samples were separated into aliquots and stored at −80°C. The gels were prepared by adding $CaCl_2$ and thrombin to activate factor XIII and convert fibrinogen to fibrin. Unless otherwise stated, the final sample composition was 1–10 mg/mL fibrinogen, 0.16 NIH U/mL thrombin, 0.14 M NaCl, 44 mM Hepes, and 2 mM $CaCl_2$ in deionized water at pH 7.4, and gelation was allowed to proceed for at least 1 h before characterization was performed. It should be noted that the addition of methionine and HOCl, which were required for the oxidation reaction, caused a negligibly small increase (<3%) in the ionic strength of the protein solutions. However, this small increase is not expected to significantly affect the fibrin gel morphology (18).

Liquid chromatography-mass spectrometry

Methionine oxidation was analyzed by nano liquid chromatography mass spectrometry (nanoLC-MS) (19). The fibrinogen was reduced with dithiothreitol, alkylated with iodoacetamide, and digested with trypsin in buffer containing 50 mM ammonium bicarbonate, 5 mM L-methionine, and 5% acetonitrile overnight at 37°C. The tryptic peptides were concentrated and desalted with C18 extraction cartridges (3M Empore), dried under vacuum, and then resuspended in solvent containing 0.1% formic acid, 5 mM L-methionine, and 5% acetonitrile. The tryptic peptides from 200 ng protein were injected for each nanoLC-MS analysis. NanoLC-MS analyses were performed in the positive ion mode with a Thermo-Finnigan LTQ linear ion trap mass spectrometer (San Jose, CA) coupled to a nanoAcquity UltraPerformance LC (UPLC) system (Waters, Milford, MA). Peptides were separated at a flow rate of 0.3 μL/min on a nanoUPLC BEH130 C18 column (100 × 0.075 mm, 1.7 μm; Waters) using 0.1% formic acid in water (solvent A) and 0.1% formic acid in CH_3CN (solvent B). Peptides were eluted using a linear gradient of 5%−35% solvent B over 90 min. The spray voltage was 2.0 kV, and the temperature of the heated capillary was 200°C. The collision energy for tandem MS (MS/MS) was 35%. Methionine oxidation was determined by the peak area from the reconstructed ion chromatograms of nonoxidized and oxidized methionine-containing peptides.

UV-Vis

UV-Vis spectroscopy measurements were made on an Evolution 300 Thermo Scientific UV-Vis spectrophotometer. Spectra over $320<\lambda<780$ nm were taken in a 1 cm path-length cell once per minute for 1 h to capture the gelation kinetics. Samples were prepared with 1 mg/mL fibrin in 0.14 M NaCl, 44 mM Hepes buffer with 0.16 NIH U/mL thrombin and 2 mM $CaCl_2$.

SEM

All SEM images were obtained on an FEI Technai (Hillsboro, OR) scanning electron microscope with a 5 kV accelerating voltage. The samples were prepared from 1 mg/mL fibrin gels, and gelation was allowed to proceed for 1 h. The gel was rinsed three times with DI-H_2O to extract excess salt. The gels were frozen at −80°C and lyophilized to preserve the structure. The samples were sputtered with a 5-nm-thick layer of gold with an SPI sputter coater.

Clot permeation and porosity

Clot permeation experiments were used to determine the average pore size in the fibrin gels as previously demonstrated in the literature (20). Fibrin gels, 8–10 mm long, containing 2.2 mg/mL 0, 50, and 150 HOCl fibrinogen with 0.16 NIH U/mL thrombin in the NaCl-Hepes buffer were prepared in Tygon tubing of 1/16 inch internal diameter. The gelation was allowed to proceed for a minimum of 1 h before measurements were obtained. The tubing with the fully formed gel was attached to a water reservoir with a 12 cm pressure head. The water was allowed to flow through the gel into a small scintillation vial for ~20 min, and the mass was measured to obtain an average flow rate.

Rheology

Rheology measurements were performed using a stress-controlled Anton Paar MCR 301 rheometer (Graz, Austria) with either a cone-and-plate configuration (25 mm diameter and 1° angle) or a concentric-cylinder configuration (16.6 mm diameter × 25 mm length and 0.71 mm gap). The temperature was maintained at 37°C with a peltier heat exchanger. Evaporation was prevented by the application of an immiscible oil layer on the exposed surface.

Gelation was monitored with 0.5% strain oscillations at 1 Hz for 1 h. Frequency sweeps were performed over $0.0005<f<50$ Hz at 0.5% strain. To measure the nonlinear rheology, the shear stress (τ) was gradually increased from 0.001 Pa to the instrument's maximum stress or until the gel broke. During the stress ramp, the strain was measured at discrete stress intervals that were logarithmically spaced.

Lysis experiments were monitored rheologically on the cone and plate using 0.5% strain oscillations at 1 Hz. The samples contained 2.2 mg/mL fibrinogen and 5 μg/mL plasminogen in standard buffer. Thrombin was added at 1.0 NIH U/mL to initiate gelation, and 0.5 μg/mL tPA was added to convert plasminogen to plasmin to initiate clot lysis. Both gelation and fibrinolysis were initiated simultaneously. However, the tPA and plasminogen were added at much lower concentration to ensure that a strong gel was formed before significant fibrinolysis occurred. Gelation and dissolution were tracked until a final plateau modulus was reached. The lysis time was defined as the point at which the modulus was only 10% higher than the final modulus value of the fully lysed sample.

tPA activation assay

The activation of plasminogen by tPA on immobilized baseline and oxidized (50μM HOCl) fibrinogen was assayed as described by Sauls et al. (21). The control and oxidized fibrinogen samples were immobilized and/or converted to fibrin with 10 nM thrombin. After immobilization, washing, and blocking, 100 μL of a mixture of 1 nM tPA, 5 μg/mL of plasminogen, and 0.1 mM Spectrozyme PCa (American Diagnostica)

(Stamford, CT) were added and the plasmin activation was monitored by absorbance of the Spectrozyme cleavage product at 405 nm at room temperature. The maximal velocity of plasmin generation was then calculated as the steepest slope of the absorbance curve. The ratios of the maximal rates of substrate cleavage between control and oxidized fibrinogen/fibrin were compared.

RESULTS

Fibrinogen oxidation

Fibrinogen was oxidized by adding HOCl at physiologically relevant concentrations between 0–150 μmol HOCl/g fibrinogen (or ~0–300 μM based on 2 mg/mL fibrinogen concentration) (22). Circular dichroism measurements were used to ensure that oxidation was not inducing measureable changes in the secondary structure of the protein. The data are reported in Fig. S1 of the Supporting Material. The extent of oxidation for several methionine residues was determined with nanoLC-MS and the results of this analysis are presented in Table 1, which shows the oxidized fraction of each selected methionine residue. In all cases, the addition of HOCl led to an increase in oxidation relative to the native fibrinogen. Three of the analyzed methionine residues (γ-78, β-367, and α-476) appear to be preferentially oxidized ($>$10% oxidation in the 50 HOCl fibrinogen and $>$30% oxidation in the 150 HOCl fibrinogen) over the remaining methionine residues. In Fig. 1, the fibrinogen crystal structure is presented with all of the methionine residues circled and the highly oxidized residues labeled (23,24). Although the crystal structure of the αC domain has not yet been fully characterized, the structure of the N-terminal subdomain has been determined by a combination of circular dichroism and NMR (25). The αC domain is included in Fig. 1 schematically with dotted lines, and the structure of the N-terminal subdomain is highlighted with the highly oxidized α-476 methionine labeled.

Gel structure

Given the physiological importance of fibrin gels and the existence of structure-driven coagulopathy, many studies have sought to characterize the structure of fibrin gels (1,17,18,23,26). Various microscopy and scattering techniques have been used to examine the structure of fibrin clots, including SEM, scanning probe microscopy, optical microscopy, SANS, small-angle x-ray scattering, and turbidity analysis. In this study, we characterized the structure of oxidized and untreated fibrin gels by using a combination of SEM, SANS, turbidity analysis, and gel permeation. Each of these techniques has various advantages and disadvantages. However, when used in combination, these techniques complement each other and provide details about the structure of the individual fibers, the gel porosity, and the network density.

TABLE 1 Oxidized fraction of selected methionine residues by HOCl with 0, 50, and 150 μM HOCl/g fibrinogen

	γ-78	α-91	α-476	β-190	β-305	β-367
0 HOCl	0.008	0.007	0.024	0.014	0.028	0.013
50 HOCl	0.112	0.010	0.256	0.052	0.043	0.137
150 HOCl	0.334	0.022	0.727	0.109	0.148	0.431

We formed fibrin gels by adding thrombin to the prepared fibrinogen samples at all three levels of oxidation. Calcium (2 mM) was added to all solutions to activate Factor XIII and promote covalent ligation. To quantify the turbidity during gelation, we measured the absorbance at λ = 350 nm of 1 mg/mL fibrin gels as a function of time and plotted it in Fig. 2. We found that the gelation time was unchanged with oxidation, which suggests that oxidation does not affect the gelation kinetics. The turbidity of the gels was highly influenced by oxidation, with the nonoxidized fibrin forming very opaque gels and the highly oxidized fibrin forming nearly transparent gels.

The turbidity of fibrin gels has long been linked to fiber diameter, with fine fibers producing clear gels (17,18). The average radius of the fibers in the 0 and 50 HOCl fibrin gels was calculated from turbidity measurements and found to be 89 nm and 75 nm, respectively. The 150 HOCl fibrin gel was too transparent to accurately measure the turbidity or determine the fiber size, but the high transparency indicates the presence of much smaller fibers. Additional details of the turbidity analysis are provided in the Supporting Material.

To ensure that the decreasing turbidity was caused by a reduction in fiber size, we had to demonstrate that these changes were not attributable to inactive fibrinogen. To that end, we added a controlled volume of buffer to the top of a fully formed gel. After ~24 h, the fibrinogen concentration in the tops was measured. We found that the baseline gel contained $<$10% inactive fibrin. The concentration of unreacted fibrin in the oxidized gels was unmeasurable, indicating that nearly all of it was activated and formed part of the clot.

SANS measurements were also used to quantify the bulk average fiber diameter in the transparent 150 HOCl fibrin gels. For SANS, a relatively high concentration (6.5 mg/mL) of fibrinogen was used to increase the scattering relative to the background. Fibrin gels from 0 and 150 HOCl fibrinogen were formed in the NaCl-Hepes buffer in H_2O. After 1 h of gelation time, the buffer was exchanged for an identical composition buffer prepared with D_2O to minimize the incoherent background and enhance the scattering contrast. The absolute scattering intensity (I) is plotted against the scattering vector (q) in Fig. S4. Additional details regarding the experimental protocol, results, and analysis of the SANS experiments are included in the Supporting Material.

From SANS we determined that the baseline fibrinogen had an average radius of 95 nm using a cylinder form factor model (29). This result is consistent with the 89 nm radius

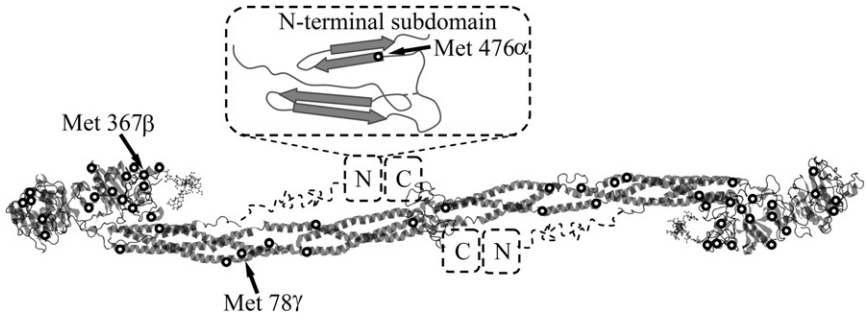

FIGURE 1 Fibrinogen molecule with all methionine residues circled and highly oxidized methionine residues labeled. The crystal structure was rendered from the Protein Data Bank (23,24). The α-C domain was added schematically with dotted lines, including the ordered N- and C-terminal subdomains (25).

calculated from the turbidity measurement. However, we found that the highly oxidized 150 HOCl fibrin gel was better represented by a bimodal distribution of fiber radii where $R_1 = 15$ nm and $R_2 = 3.4$ nm. Although the bimodal model fit was very good, there is significant uncertainty in the absolute value of the radii. In fact, the small radius determined from the fit is slightly less than is typically reported for a single protofibril (~5 nm) (27). Regardless, these results are consistent with both the SEM results reported below and the turbidity data suggesting that very small fibers exist in the highly oxidized gels.

Fibrin gels were also prepared from 1 mg/mL fibrinogen for SEM analysis. In Fig. 3 SEM images at 1000 and 20,000× magnification are presented for oxidized and untreated fibrin. Additional images at 10,000 and 50,000× are included in Fig. S2. In the 1000× magnified images, it is clear that the network density increases dramatically with increasing oxidation. In the nonoxidized fibrin gel, very large fibers are separated by longer distances, giving rise to large pores in the gel. In the 50 HOCl oxidized fibrin gel, the fiber and pore sizes are reduced relative to the nonoxidized gel, but the most dramatic difference is observed in the 150 HOCl fibrin gel. This gel primarily contained densely packed but very small fibers. It should be noted that in the 150 HOCl oxidized fibrin gels, the fibers were so closely packed in the bulk of gel that the sputtered gold obscured the individual fibers. For this reason, these images were taken near the edge of the gel where the fiber density was much lower. It is expected that the high fiber density and reduced porosity observed in the oxidized fibrin gels would lead to reduced diffusivity through the gel and impede the transport of enzymes critical for fibrinolysis.

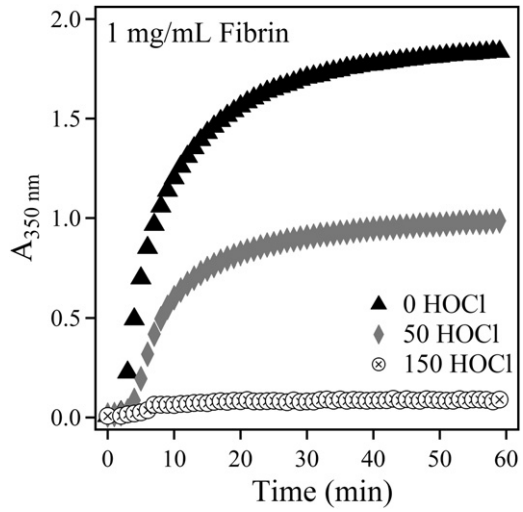

FIGURE 2 Absorbance at 350 nm for 1 mg/mL fibrin gels plotted as a function of time during gelation.

The pore size in 2.2 mg/mL gels was quantified with a gel permeation study similar to the one described by Carr and Hardin (20). Darcy's constant (Da), which is related to the gel porosity, is defined by Eq. 1:

$$Da = \frac{V\eta h}{AtP} \tag{1}$$

where V is the volume of water that passes through the gel in time (t), η is the viscosity of water, h is the length of the fibrin clot plug, A is the cross-sectional area of the tube, and P is the water pressure head. The average pore size (R_P) can be obtained from a relation derived by Carr and Hardin (20):

$$R_P = \frac{0.5093}{Da^{-1/2}} \tag{2}$$

The results of this study indicate that there is a decrease in the pore size with increasing oxidation. The 0, 50, and 150 HOCl fibrin gels have average pore radii of 540, 370, and 230 nm, respectively, based on the gel permeation measurements.

Rheology

The multiscale structure of fibrin gels gives rise to interesting linear and nonlinear mechanical properties that are critical for the function of fibrin clots in vivo. Altered mechanical properties reflect changes in clot structure, and measurements of these properties are often used as a diagnostic tool for coagulopathy. Typically the mechanical properties of fibrin gels are measured by means of shear rheology (in research) or thromboelastography (in clinical applications) (2,30). In shear rheology, the structure of

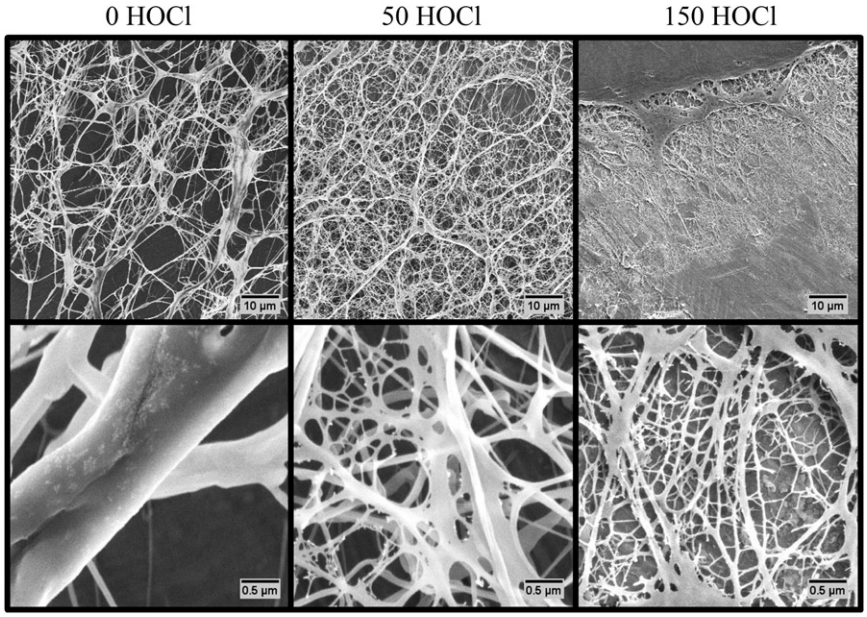

FIGURE 3 SEM images of fibrin gels from HOCl oxidized fibrinogen at 1000× (*top*) and 20,000× (*bottom*) magnification.

a clot is informed by various models for the linear and nonlinear elastic modulus as a function of concentration or strain (31–33). Given the vast number of physiological modifications that human fibrinogen can undergo, mechanical measurements are a powerful tool for detecting abnormal fibrin coagulation.

In this study, we measured the mechanical properties of the fibrin gels using shear rheology techniques. At low strain (<1%), the fibrin gels were below the linear viscoelastic limit. Small-amplitude oscillations at strains within the linear viscoelastic limit were used to track the evolving elastic (G') and viscous (G'') moduli during gelation. The viscous and elastic moduli are plotted as a function of time in Fig. 4. As with the UV-Vis measurements, we found

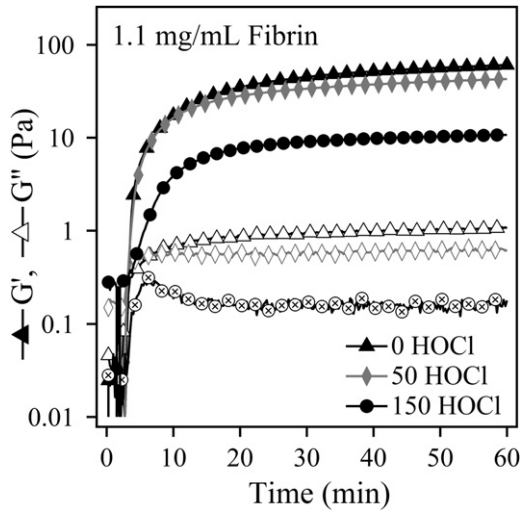

FIGURE 4 Elastic (G′) and viscous (G″) moduli of oxidized and baseline fibrin gels plotted as a function of time during gelation.

no significant changes in the gelation time, and in all three cases the modulus had increased only slightly at the end of the 1 h gelation period. A frequency sweep between 0.0005 and 50 Hz was also performed and data from these measurements are reported in Fig. S6. All of the samples, oxidized and baseline, have gel-like properties, with $G' > G''$ over the entire frequency range that was probed. This is typical for cross-linked fibrin at the concentrations probed in this study.

In Fig. 5, we examine the concentration dependence of the linear elastic modulus. The elastic modulus at 0.5% strain is plotted over a concentration range spanning two decades. We find that the oxidized gels are systematically weaker than the baseline gels, but the overall concentration dependence is effectively the same. The linear elastic modulus is found to vary exponentially with fibrinogen concentration such that G' increases as $C^{2.12}$, $C^{2.32}$, and $C^{2.35}$ for the 0, 50, and 150 HOCl fibrin gels, respectively. The variation in the exponential dependence is thought to be a result of experimental error rather than an indication of any underlying structural changes.

MacKintosh et al. (31) proposed a model that predicts that the linear elastic modulus of entangled biopolymer networks should have an exponential concentration dependence with $G' \sim C^{2.2}$. Various experimental studies have reported an exponential dependence for cross-linked fibrin ranging between $G' \sim C^{1.66}$ and $G' \sim C^{2.3}$ (2,26,31,34). The values reported herein are consistent with those results. Additionally, we used SDS-PAGE to demonstrate that covalent cross-linkage by Factor XIIIa is not inhibited by HOCl oxidation. A scan of the gel is presented in Fig. S5. The 115 kD γ-γ dimers (γ_2) are prominent in both the oxidized and native fibrin samples and are indicative of covalent cross-linkage via Factor XIIIa. This is clear evidence that Factor

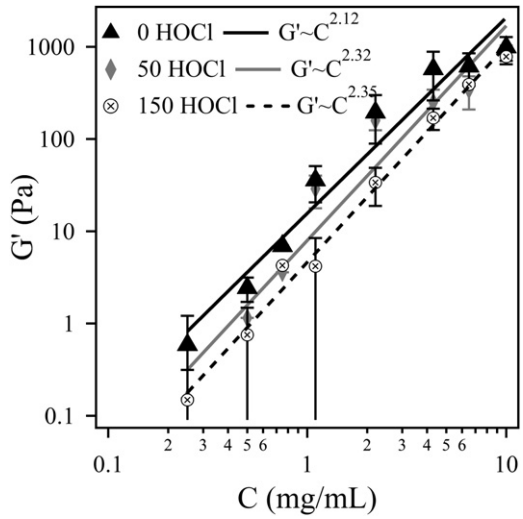

FIGURE 5 Linear elastic modulus of the fibrin gels plotted against the fibrinogen concentration.

XIII activation by thrombin and the activity of Factor XIIIa are not impaired by HOCl oxidation.

Fibrin gels are also known to exhibit highly nonlinear strain-hardening mechanical properties. To measure the nonlinear rheology of the oxidized fibrin gels, we applied a continuously increasing stress ramp until the gel failed, and measured the resulting strain at discrete stress intervals. It should be noted, however, that all of the 6.5 mg/mL fibrin gels and some of the 4.3 mg/mL fibrin gels were too strong to break in the rheometer. We determined the instantaneous modulus (G_{Inst}) by taking the derivative of the shear stress (τ) with respect shear strain (γ):

$$G_{Inst} = \frac{d\tau}{d\gamma} \tag{3}$$

Curves of the average instantaneous modulus for 1.1, 2.2, 4.3, and 6.5 mg/mL fibrin gels formed from baseline and oxidized fibrinogen are plotted in Fig. 6. The error bars reflect the standard deviation from a minimum of three different gels.

The nonlinear rheology of fibrin is related to the underlying hierarchical structure of the clot and therefore is affected by alterations to the monomer. Like many biopolymers, fibrin gels are highly extensible and exhibit strain hardening (32,33,35). In this study, all of the fibrin gels we tested strain hardened regardless of concentration or oxidation levels. The instantaneous modulus at the maximum strain before gel failure was typically 1–2 orders of magnitude greater than the linear elastic modulus. We consistently found that the maximum strain and maximum modulus were lower for oxidized gels than for baseline gels. For the 1 mg/mL gels, the average maximum strain before failure was 202 ± 31, 143 ± 10, and 157 ± 20% for 0, 50, and 150 HOCl gels, respectively. The average

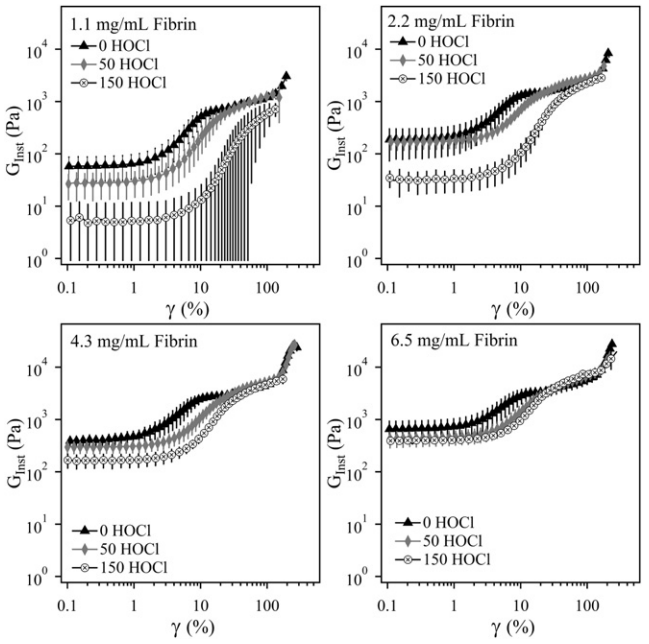

FIGURE 6 Instantaneous modulus (G_{Inst}) of fibrin gels with various concentrations of fibrinogen and oxidized to different levels with 0, 50, and 150 μmol HOCl/g fibrinogen. The data plotted are the average of at least three trials, with error bars corresponding to the standard deviation.

maximum modulus reached before gel failure was 3000 ± 1500, 1400 ± 100, and 800 ± 200 Pa, respectively. Although the linear elastic moduli and maximum instantaneous moduli of the oxidized gels were lower than those measured in the baseline gels, at intermediate strains (approaching 100%), the magnitude of the instantaneous modulus of the baseline and oxidized gels began to equalize. All of the baseline gels experienced a second increase in the magnitude of strain hardening at very high strain. This upturn also occurred in the higher-concentration 50 HOCl gels and the 6.5 mg/mL 150 HOCl gel.

The limit of linear viscoelasticity of the gels was also affected by HOCl oxidation. We found that the onset of strain hardening occurred at progressively higher strain with increasing oxidation. We quantified the delayed strain hardening by measuring the strain at which the instantaneous modulus reached 200% of the linear modulus. This characteristic strain was found to be 3.6 ± 0.6, 5.5 ± 1.5, and 7.5 ± 1.1% for 0, 50, and 150 HOCl fibrin gels, respectively, when averaged over all concentrations. The linear viscoelastic limit also increased slightly with concentration, which is consistent with current models for strain hardening (33,36).

Clot lysis

HOCl oxidation has been implicated in altered fibrinolysis in at least one previous report (15). Given the altered clot structure and rheology observed in this study, we expected

to find delayed fibrinolysis in the oxidized fibrin gels as a result of reduced diffusivity of enzymes and cofactors through smaller pores. From the gel permeation experiments, we measured the pore size of the gels to be 540 nm for untreated fibrinogen, 370 nm for the 50 HOCl oxidized fibrinogen, and 231 nm for the 150 HOCl oxidized fibrinogen in 2.2 mg/mL fibrin gels. The Stokes radius of plasminogen is ~5 nm (37). The diffusion coefficient for plasminogen at infinite dilution in water (D_{AB}) can be calculated from the Stokes-Einstein equation:

$$D_{AB} = \frac{kT}{6\pi R\mu_B} \tag{4}$$

where k is the Boltzmann's coefficient, T is the temperature, R is the radius of plasminogen, and μ_B is the viscosity of water ($D_{AB} = 6.49 \times 10^{-11}$ m^{2}s^{-1} at 37°C).

In the case of plasminogen diffusing through a fibrin gel, the added restriction to diffusion imposed by the fiber network must be considered. Two correction factors, the steric partition coefficient ($F_1(\varphi)$) and the hydrodynamic hindrance factor ($F_2(\varphi)$), are used to account for this effect, such that an effective diffusion coefficient for plasminogen through the fibrin gel (D_{AF}) can be calculated with the following equation (38):

$$D_{AF} = D_{AB}F_1(\varphi)F_2(\varphi) \tag{5}$$

Both of these parameters are functions of the reduced pore diameter (φ):

$$\varphi = \frac{d_{plasminogen}}{d_{pore}} \tag{6}$$

where $d_{plasminogen}$ is the diameter of the plasminogen protein, and d_{pore} is the estimated pore diameter. The steric partition coefficient accounts for the volume occupied by the plasminogen because it cannot be located closer than one radius away from the pore wall. This factor was originally derived using geometric arguments and is defined in Eq. 7 (38):

$$F_1(\varphi) = (1-\varphi)^2 \tag{7}$$

The hydrodynamic hindrance factor accounts for the hindered Brownian motion of plasmin within the pore volume. The hydrodynamic hindrance factor developed by Renkin (39) for hard spheres diffusing through cylindrical pores is valid for $0 < \varphi < 0.6$. Although the pores in the fibrin gels are not cylindrical and the plasminogen is not a hard sphere, Eq. 8 still remains a reasonable approximation for the hydrodynamic hindrance factor in this system:

$$F_2(\varphi) = 1 - 2.104\varphi + 2.09\varphi^3 - 0.95\varphi^5 \tag{8}$$

Given the calculated pore sizes for fibrin gels with and without oxidation, the effective diffusion coefficients of plasminogen in gels are found to be 5.8×10^{-11}, 5.5×10^{-11}, and 4.9×10^{-11} m^{2}s^{-1} for the 0, 50, and 150 HOCl gels, respectively. Based on these calculated diffusion coefficients, we expect that the lysis time for oxidized fibrin gels will be affected by reduced porosity in the oxidized gels.

We performed a series of fibrinolysis experiments using the rheometer with small-amplitude shear oscillations to monitor the elastic and viscous moduli during gelation, and the subsequent lysis of fibrin gels in situ. In this experiment, 2.2 mg/mL fibrinogen and 1 μg/mL plasminogen were combined with 1 NIH U/mL thrombin and 0.5 μg/mL tPA, and loaded directly into the rheometer using the cone-and-plate geometry. We determined the lysis time by taking the time at which the elastic modulus reached a value that was just 10% larger than the final plateau elastic modulus. The results of this experiment are presented in Fig. 7, with the lysis time of the representative data sets indicated by arrows. We found that, as expected, the lysis time was delayed in oxidized gels.

Fibrin is known to increase the rate of tPA-induced conversion of plasminogen to plasmin by increasing exposure of tPA-binding sites (40). In a comparison of fibrinogen with fibrin, tPA-induced plasmin activation is typically increased by a ratio of ~1:1.5–2. We also anticipated that fibrinogen oxidation could decrease the rate of tPA-dependent plasminogen activation. However, both control and oxidized fibrin/fibrinogen plasminogen activation ratios were similar (1.60 vs. 1.66, respectively), leading us to conclude that the rate of tPA-induced activation of plasminogen

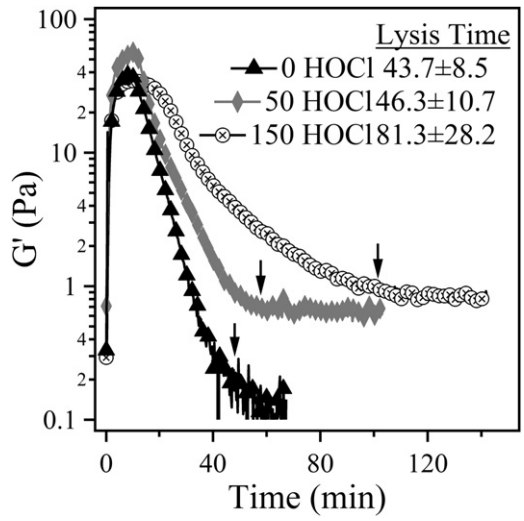

FIGURE 7 Fibrinolysis induced by tPA and plasminogen in 2.2 mg/mL fibrin gels formed from fibrinogen treated with 0, 50, and 150 μmol/g fibrinogen as monitored by small-amplitude oscillatory rheology. The lysis time for these specific gels is marked with an arrow. The reported lysis times represent the average of three trials.

is essentially unchanged by the presence of oxidized fibrin. Therefore, the delayed lysis time is likely to be primarily attributed to changes in clot architecture and diffusion.

DISCUSSION AND CONCLUSIONS

Fibrinogen treatment with HOCl leads to the preferential oxidation of specific methionine residues on the α, β, and γ chains. The oxidation of one or all of these residues is associated with reduced lateral aggregation of protofibrils resulting in gels with smaller fibers and higher fiber density compared with untreated fibrin gels. Both the linear and nonlinear mechanical properties are affected by oxidation. Oxidized fibrin gels are weaker and experience a delayed onset of strain hardening.

High fiber density as a result of fine fiber formation is thought to reduce the diffusion rate of plasminogen through the gel and lead to prolonged lysis times. Several medical conditions associated with thrombosis, including diabetes and impaired kidney function, have been associated with these characteristics (7,8). The results presented in this study suggest that oxidation related to neutrophil activation and inflammation may be associated with these diseases (10,11). Moreover, in this work we demonstrate that the delayed lysis observed in these oxidized gels is not a result of decreased tPA-dependent activation of plasminogen, but rather may be explained by a reduction in gel porosity and hindered diffusion of the plasminogen through the clot.

These results support an oxidative modification of fibrin polymerization, as previously reported (41). Although the exact mechanism of altered fibrin polymerization remains unclear, several studies have demonstrated inhibited lateral aggregation of protofibrils through the manipulation of the α-C domains (42–45). Removal of the α-C domain or substitution with chicken α-C domains inhibits lateral aggregation and results in clots similar to ours with higher fiber density, weaker gels, and prolonged fibrinolysis times (43,44). The distinct similarities between the abnormal coagulation observed with the α-C domain variants and our results suggest that perhaps oxidation via HOCl acts by promoting a conformational change in the α-C domain that inhibits interactions with adjacent domains during fibrin fiber polymerization.

The most preferentially oxidized methionine residue is α-476, with 2.4%, 25.6%, and 72.7% oxidized in the 0, 50, and 150 HOCl solutions, respectively. This methionine is the first residue on a second β-sheet hairpin complex in the N-terminal subdomain of the α-C domain. Tsurupa and colleagues (25) found that this second β-sheet hairpin is relatively unstable in human fibrinogen and that the unfolding of this structure reduces the extent of α-C fragment oligomerization. Although we present no conclusive evidence demonstrating that conformational changes in the α-C domain lead to the impaired lateral aggregation of protofibrils in oxidized fibrin gels, our results in conjunction with recent literature do suggest that oxidation of the methionine residue α-476 could be, at least in part, responsible for the altered clotting of HOCl oxidized fibrin gels. This work highlights the need for further studies of the effect of specific residue oxidation on the conformation and oligomerization of the α-C domain.

SUPPORTING MATERIAL

Six figures and one table are available at http://www.biophysj.org/biophysj/supplemental/S0006-3495(12)01189-7.

Part of this work was conducted at the University of Washington NanoTech User Facility, a member of the National Nanotechnology Infrastructure Network, National Science Foundation (NSF). The MS experiments were performed by the Mass Spectrometry Core, Puget Sound Blood Center Research Institute. This work was supported by the University of Washington Royalty Research Fund and grant KL2 TR000421 to N.W. from the National Center for Advancing Translational Sciences (NCATS), a component of the National Institutes of Health (NIH). Its contents are solely the responsibility of the authors and do not necessarily represent the official view of NCATS or NIH. This work utilized facilities supported in part by the National Science Foundation under Agreement No. DMR-0944772. The National Institute of Standards and Technology, U.S. Department of Commerce, provided the neutron research facilities used in this work. This work benefitted from software developed by the DANSE project under NSF award DMR-0520547.

REFERENCES

1. Doolittle, R. F. 1984. Fibrinogen and fibrin. *Annu. Rev. Biochem.* 53:195–229.
2. Ryan, E. A., L. F. Mockros, …, L. Lorand. 1999. Structural origins of fibrin clot rheology. *Biophys. J.* 77:2813–2826.
3. Yang, Z., I. Mochalkin, and R. F. Doolittle. 2000. A model of fibrin formation based on crystal structures of fibrinogen and fibrin fragments complexed with synthetic peptides. *Proc. Natl. Acad. Sci. USA.* 97:14156–14161.
4. Pretorius, E., H. Steyn, …, H. M. Oberholzer. 2011. Differences in fibrin fiber diameters in healthy individuals and thromboembolic ischemic stroke patients. *Blood Coagul. Fibrinolysis.* 22:696–700.
5. Colle, J. P., Z. Mishal, …, C. Soria. 1999. Abnormal fibrin clot architecture in nephrotic patients is related to hypofibrinolysis: influence of plasma biochemical modifications: a possible mechanism for the high thrombotic tendency? *Thromb. Haemost.* 82:1482–1489.
6. Jorneskog, G., K. Fatah, and M. Blomback. 1998. Fibrin gel structure in diabetic patients before and during treatment with acetylsalicylic acid: a pilot study. *Fibrinolysis Proteolysis.* 12:360–365.
7. Henschen-Edman, A. H. 2001. Fibrinogen non-inherited heterogeneity and its relationship to function in health and disease. *Ann. N. Y. Acad. Sci.* 936:580–593.
8. Shacter, E., J. A. Williams, …, R. L. Levine. 1994. Differential susceptibility of plasma proteins to oxidative modification: examination by western blot immunoassay. *Free Radic. Biol. Med.* 17:429–437.
9. Stief, T. W., J. Kurz, …, J. Fareed. 2000. Singlet oxygen inactivates fibrinogen, factor V, factor VIII, factor X, and platelet aggregation of human blood. *Thromb. Res.* 97:473–480.
10. Hazen, S. L., F. F. Hsu, …, J. W. Heinecke. 1996. Human neutrophils employ chlorine gas as an oxidant during phagocytosis. *J. Clin. Invest.* 98:1283–1289.
11. Shao, B., A. Belaaouaj, …, J. W. Heinecke. 2005. Methionine sulfoxide and proteolytic cleavage contribute to the inactivation of cathepsin G

by hypochlorous acid: an oxidative mechanism for regulation of serine proteinases by myeloperoxidase. *J. Biol. Chem.* 280:29311–29321.

12. Pattison, D. I., C. L. Hawkins, and M. J. Davies. 2007. Hypochlorous acid-mediated protein oxidation: how important are chloramine transfer reactions and protein tertiary structure? *Biochemistry.* 46:9853–9864.
13. Nalian, A., and A. V. Iakhiaev. 2008. Possible mechanisms contributing to oxidative inactivation of activated protein C: molecular dynamics study. *Thromb. Haemost.* 100:18–25.
14. Glaser, C. B., J. Morser, J. H. Clarke, E. Blasko, K. McLean, I. Kuhn, R. J. Chang, J. H. Lin, L. Vilander, W. H. Andrews…, 1992. Oxidation of a specific methionine in thrombomodulin by activated neutrophil products blocks cofactor activity. A potential rapid mechanism for modulation of coagulation. *J. Clin. Invest.* 90:2565–2573.
15. Stief, T. W. 2007. Singlet oxygen potentiates thrombolysis. *Clin. Appl. Thromb. Hemost.* 13:259–278.
16. Collet, J. P., D. Park, …, J. W. Weisel. 2000. Influence of fibrin network conformation and fibrin fiber diameter on fibrinolysis speed: dynamic and structural approaches by confocal microscopy. *Arterioscler. Thromb. Vasc. Biol.* 20:1354–1361.
17. Carr, Jr., M. E., and J. Hermans. 1978. Size and density of fibrin fibers from turbidity. *Macromolecules.* 11:46–50.
18. Yeromonahos, C., B. Polack, and F. Caton. 2010. Nanostructure of the fibrin clot. *Biophys. J.* 99:2018–2027.
19. Fu, X., J. Chen, …, J. A. López. 2011. Shear stress-induced unfolding of VWF accelerates oxidation of key methionine residues in the A1A2A3 region. *Blood.* 118:5283–5291.
20. Carr, Jr., M. E., and C. L. Hardin. 1987. Fibrin has larger pores when formed in the presence of erythrocytes. *Am. J. Physiol.* 253:H1069–H1073.
21. Sauls, D. L., E. Lockhart, …, M. Hoffman. 2006. Modification of fibrinogen by homocysteine thiolactone increases resistance to fibrinolysis: a potential mechanism of the thrombotic tendency in hyperhomocysteinemia. *Biochemistry.* 45:2480–2487.
22. Kalyanaraman, B., and P. G. Sohnle. 1985. Generation of free radical intermediates from foreign compounds by neutrophil-derived oxidants. *J. Clin. Invest.* 75:1618–1622.
23. Kollman, J. M., L. Pandi, …, R. F. Doolittle. 2009. Crystal structure of human fibrinogen. *Biochemistry.* 48:3877–3886.
24. Berman, H., K. Henrick, and H. Nakamura. 2003. Announcing the worldwide Protein Data Bank. *Nat. Struct. Biol.* 10:980.
25. Tsurupa, G., R. R. Hantgan, …, L. Medved. 2009. Structure, stability, and interaction of the fibrin(ogen) αC-domains. *Biochemistry.* 48:12191–12201.
26. Weigandt, K. M., D. C. Pozzo, and L. Porcar. 2009. Structure of high density fibrin networks probed with neutron scattering and rheology. *Soft Matter.* 5:4321–4330.
27. Janmey, P. A., J. P. Winer, and J. W. Weisel. 2009. Fibrin gels and their clinical and bioengineering applications. *J. R. Soc. Interface.* 6:1–10.
28. Reference deleted in proof.
29. Lindner, P. 2004. Neutrons, X-rays, and Light: Scattering Methods Applied to Soft Condensed Matter. Elsevier, Amsterdam.
30. Nielsen, V. G., B. M. Cohen, and E. Cohen. 2005. Effects of coagulation factor deficiency on plasma coagulation kinetics determined via thrombelastography: critical roles of fibrinogen and factors II, VII, X and XII. *Acta Anaesthesiol. Scand.* 49:222–231.
31. MacKintosh, F. C., J. Käs, and P. A. Janmey. 1995. Elasticity of semiflexible biopolymer networks. *Phys. Rev. Lett.* 75:4425–4428.
32. Storm, C., J. J. Pastore, …, P. A. Janmey. 2005. Nonlinear elasticity in biological gels. *Nature.* 435:191–194.
33. Onck, P. R., T. Koeman, …, E. van der Giessen. 2005. Alternative explanation of stiffening in cross-linked semiflexible networks. *Phys. Rev. Lett.* 95:178102.
34. Janmey, P. A., U. Euteneuer, …, M. Schliwa. 1991. Viscoelastic properties of vimentin compared with other filamentous biopolymer networks. *J. Cell Biol.* 113:155–160.
35. van Dillen, T., P. R. Onck, and E. Van der Giessen. 2008. Models for stiffening in cross-linked biopolymer networks: A comparative study. *J. Mech. Phys. Solids.* 56:2240–2264.
36. Kang, H., Q. Wen, …, F. C. MacKintosh. 2009. Nonlinear elasticity of stiff filament networks: strain stiffening, negative normal stress, and filament alignment in fibrin gels. *J. Phys. Chem. B.* 113:3799–3805.
37. Marshall, J. M., A. J. Brown, and C. P. Ponting. 1994. Conformational studies of human plasminogen and plasminogen fragments: evidence for a novel third conformation of plasminogen. *Biochemistry.* 33:3599–3606.
38. Wicks, C. E., W. R. Welty, …, G. L. Rorrer. 2008. Fundamentals of Momentum, Heat, and Mass Transfer. John Wiley & Sons, New York.
39. Renkin, E. M. 1954. Filtration, diffusion, and molecular sieving through porous cellulose membranes. *J. Gen. Physiol.* 38:225–243.
40. Nieuwenhuizen, W. 2001. Fibrin-mediated plasminogen activation. *Ann. N. Y. Acad. Sci.* 936:237–246.
41. Shacter, E., J. A. Williams, and R. L. Levine. 1995. Oxidative modification of fibrinogen inhibits thrombin-catalyzed clot formation. *Free Radic. Biol. Med.* 18:815–821.
42. Weisel, J. W., and L. Medved. 2001. The structure and function of the αC domains of fibrinogen. *Ann. N. Y. Acad. Sci.* 936:312–327.
43. Collet, J.-P., J. L. Moen, …, J. W. Weisel. 2005. The αC domains of fibrinogen affect the structure of the fibrin clot, its physical properties, and its susceptibility to fibrinolysis. *Blood.* 106:3824–3830.
44. Ping, L., L. Huang, …, S. T. Lord. 2011. Substitution of the human αC region with the analogous chicken domain generates a fibrinogen with severely impaired lateral aggregation: fibrin monomers assemble into protofibrils but protofibrils do not assemble into fibers. *Biochemistry.* 50:9066–9075.
45. Tsurupa, G., A. Mahid, …, L. Medved. 2011. Structure, stability, and interaction of fibrin αC-domain polymers. *Biochemistry.* 50:8028–8037.